
Extended X-Ray Absorption Fine Structure Measurements of Laser Shocks in Ti and V and Phase Transformation in Ti

Introduction

Recently, x-ray diffraction has been used to study dynamic material response to shocks of high pressure (~ 0.1 to 1 Mbar) and high strain rate ($\sim 10^7$ to 10^8 s $^{-1}$).¹⁻³ The goal of this work is to demonstrate the use of extended x-ray absorption fine structure (EXAFS)⁴ as a complementary characterization of such laser-shocked metals. EXAFS is the modulation in the x-ray absorption above the K edge (or L edge) due to the interference of the photoelectron wave packet with the waves reflected from neighboring atoms. Unlike synchrotron experiments where the imposed temperature is known independently and the main emphasis is on the study of the chemical structure, in this experiment the emphasis is on the measurement of the compression and temperature of the shocked material through the EXAFS spectrum itself. The frequency of EXAFS modulations is related to the interparticle distance, hence to the compression. The damping rate of the modulation can yield the lattice temperature, *which is not available by other methods*. The assumption of three-dimensional compression, required to relate the EXAFS-determined inter-atomic distance to the density, was verified by comparison with measurements of the shock speed, which yield the compression (through the known Hugoniot equation of state).

EXAFS measurements were performed on vanadium and titanium shocked to ~ 0.5 Mbar with a 3-ns laser pulse. The radiation source for the EXAFS measurement was obtained by imploding a spherical target using the 60-beam OMEGA laser.⁵ For vanadium (where no phase transformation exists below ~ 1 Mbar) the measurements demonstrate that EXAFS is a useful method for measuring the compression and temperature of sub-Mbar shocks. For Ti, where an α -Ti to ω -Ti crystal phase transformation is known to occur around ~ 0.1 Mbar, over longer time scales (μ s) behind a steady shock,^{6,7} the measurements show that EXAFS can be used to study such transformations over subnanosecond time scales.

In a previous paper⁸ we showed that a CH shell imploded by a multibeam laser system constitutes a ~ 120 -ps source of intense and relatively smooth spectrum of x-ray radiation,

suitable for EXAFS measurements. Using the 60-beam OMEGA laser, the measured room-temperature Ti EXAFS spectrum agreed with synchrotron results under similar conditions.

The subject of laser-shocked metals can be viewed from two complementary points of view: as a problem in solid-state physics and/or as a problem in plasma physics. The EXAFS measurements in this experiment, and particularly the diffraction measurements¹⁻³ of similar laser shocks, indicate that laser-shocked metals for pressures under ~ 1 Mbar largely retain their crystal-order properties. This is why the crystal phase transformation in Ti could be demonstrated with laser-driven shock waves. The shock dynamics have been simulated with a plasma-physics hydrodynamic code (see **Hydrodynamic Simulations**). The laser-deposition region where the shock is generated is certainly a plasma region and can be simulated only with a plasma-physics code. However, the same code is used to simulate both shock generation and propagation through the sample, thus relating the incident laser intensity to the resulting shock strength. The hydrodynamic code can well simulate the compressed solid because the semi-empirical equation of state⁹ is normalized to known experimental properties of the metal (such as specific heat, Grüneisen parameter, and bulk modulus). The comparison of the code and experimental results forms the basis for the study of the compressed solid, which apart from its crystalline order is also a high-density or strongly coupled plasma. Such plasmas are of great interest in understanding the interior of planets and the behavior of matter under extreme conditions.

Experimental

Figure 97.14 shows a schematic view of the target used to measure EXAFS spectra in laser-shocked targets. Of the 60 OMEGA laser beams, 57 beams of ~ 21 -kJ total energy are focused on an empty CH shell whose implosion generates the radiation source for measuring the absorption spectrum in V or Ti. In previous laser-based EXAFS experiments^{10,11} a planar high-Z target was used where the spectrum was dominated by spectral-line emission and was thus not smooth. The low-Z imploding target used here produces a very intense and smooth

continuum spectrum,⁸ appropriate for absorption measurements. The three remaining OMEGA beams are stacked and used to launch a planar shock wave in the metal target. The laser pulse shape was 1 ns square (each of energy ~50 J); thus the three-stacked beams formed a 3-ns-long square pulse. These beams were focused onto the planar target in a 3.8-mm-diam focal spot, giving an irradiance of 0.4 to 0.5 TW/cm². The delay time of the three-stacked beams with respect to the remainder of the beams was adjusted so that peak implosion (and emission) of the spherical target occurred when the shock wave had just exited the metal layer. The spherical target had a diameter ~950 μm and a CH wall thickness ~20 μm. The planar target consisted of 10-μm-thick polycrystalline V or Ti, coated on both sides with a 17-μm-thick CH layer. The purpose of the front CH layer was to prevent laser heating and ablation of the metal. The purpose of the back CH layer was to prevent shock unloading at the back metal surface. The heat shield (0.5-mm-thick CH foil) minimizes the heating of the metal layer due to soft radiation from the imploding spherical target.

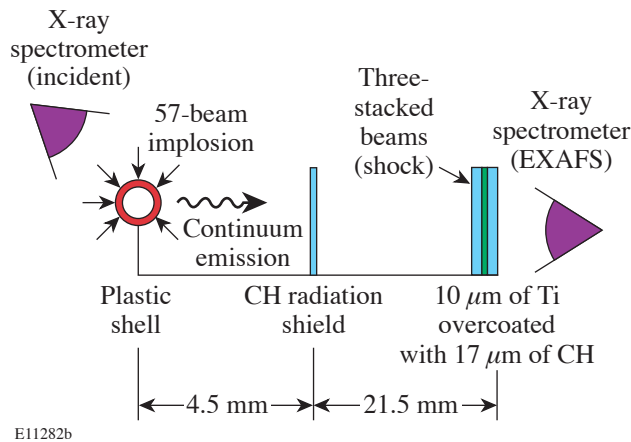


Figure 97.14 Schematic view of the experimental configuration. The imploding spherical target serves as a radiation source for EXAFS measurements. The three-stacked beams launch a shock through the Ti (or V) layer.

Two cross-calibrated x-ray spectrometers measured the spectrum on calibrated film. One spectrometer measured the EXAFS spectrum, the other the incident spectrum. The spectra were measured simultaneously on a single target shot. A typical record of the transmitted spectrum showing EXAFS modulation is shown in Fig. 97.15. As explained in Ref. 8, the high incident intensity enabled us to choose a relatively thick sample (giving an optical depth of 3.5 just above the Ti *K*

edge), which yields high relative modulation amplitude in the measured spectrum. However, the spectrum below the *K* edge is then saturated; to accurately determine the *K*-edge position and below-the-edge signal intensity, we used an Al attenuator on part of the entrance slit, as seen in Fig. 97.15. A typical incident spectrum is shown in Fig. 2(a) of Ref. 8. The spectral resolution of the spectrometer, limited by the source size, was ~5 eV, much smaller than a typical EXAFS modulation period (~60 eV).

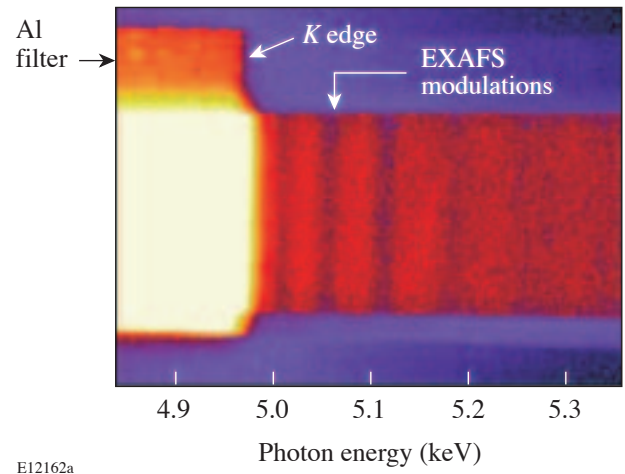


Figure 97.15 Typical record of the transmitted spectrum (from unshocked Ti) showing EXAFS modulations above the *K* edge.

Although the EXAFS measurement is time integrated, a meaningful shock diagnosis can be obtained without streaking the spectrum in time because the x-ray pulse width is ~120 ps,⁸ much shorter than the shock transit time through the metal (~2 ns). The timing of the shock relative to the implosion-induced backlighter pulse was measured by the method of active shock breakout (ASBO),¹² a method that uses a frequency-doubled YAG laser probe, reflected from the backside of the target. Figure 97.16 shows a schematic of the setup and a typical streak result; $\tau(\text{Ti})$ and $\tau(\text{CH})$ are the times when the shock has traversed the metal layer and the back CH layer, respectively. This measurement determines the correct timing between the implosion beams and shock-producing beams. It also yields the shock speed in the metal (~5 μm/ns), from which, using the known Hugoniot equation of state, the shock compression and pressure can be obtained. Finally, images such as in Fig. 97.16 indicate a lateral nonuniformity (due to the laser's focal-spot distribution) of ±10% in the shock speed, thus also in the shock compression.

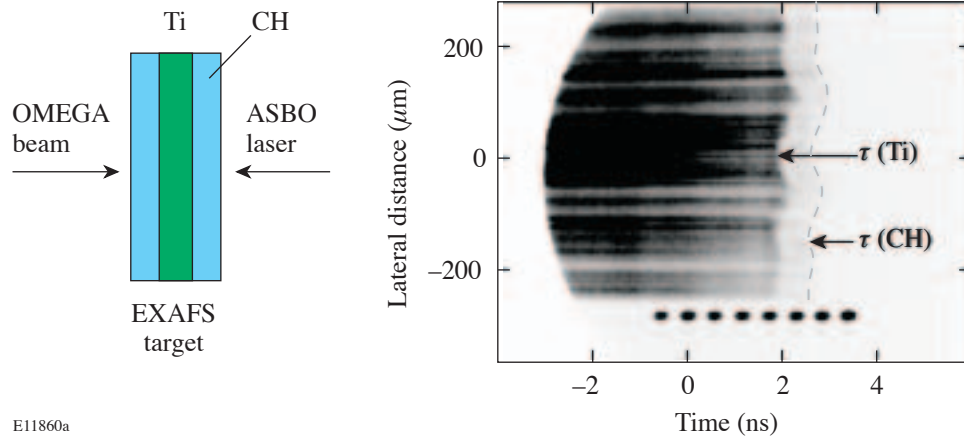


Figure 97.16

Schematic and a typical streak of the ASBO probe beam reflected from the backside of the target. $\tau(\text{Ti})$ and $\tau(\text{CH})$ are the times when the shock exits the metal layer and the back CH layer, respectively. This measurement provides (a) the correct timing between the capsule-implosion beams and shock-producing beams, (b) the shock speed in the metal, and (c) the lateral shock uniformity.

Hydrodynamic Simulations

The expected shock strength and the properties of the shocked vanadium and titanium were determined using one-dimensional simulations with the hydrodynamic code *LASNEX*.¹³ The profiles of pressure, density, and temperature versus position are shown for V in Fig. 97.17 and for Ti in Fig. 97.18, at the time of arrival of the shock at the rear surface of the metal layer for an incident laser intensity of $\sim 0.5 \text{ TW/cm}^2$. The range (around the volume average) of parameter values within the V layer is (1) pressure: $0.43 \pm 0.03 \text{ Mbar}$; (2) temperature: $980 \pm 160 \text{ K}$; and (3) volume compression: 1.19 ± 0.05 . These variations in the axial direction are larger than the lateral variations due to laser nonuniformity; for this reason a one-dimensional simulation of the shocked metals is adequate. For Ti the comparable ranges are (1) pressure: $0.33 \pm 0.05 \text{ Mbar}$; (2) temperature: $900 \pm 130 \text{ K}$; and (3) volume compression: 1.2 ± 0.06 . The EXAFS measurements (in the case where the metals were shocked) are averaged over the shocked volume; thus, the volume averages are the appropriate theoretical quantities to compare with the experiment.

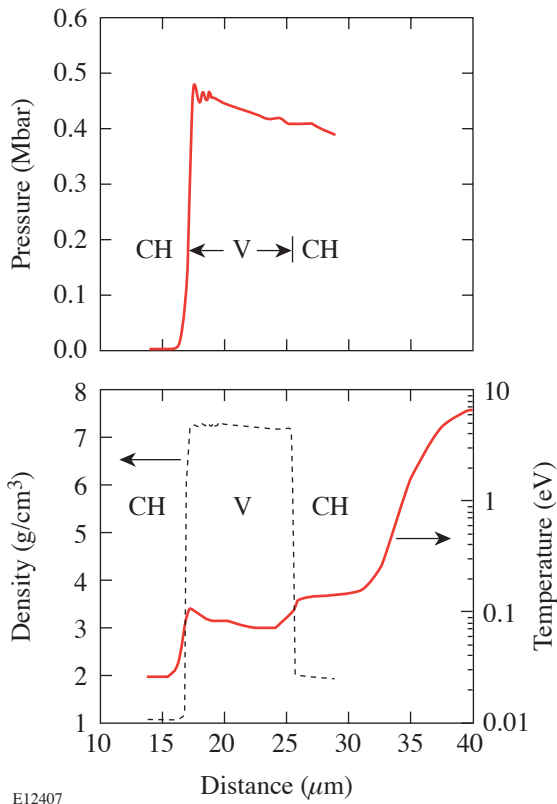
Theory

The measured spectra were analyzed with the *FEFF8 ab initio* EXAFS software package.¹⁴ The basic theory of EXAFS⁴ yields an expression for the relative absorption $\chi(k) = \mu(k)/\mu_0(k) - 1$, where $\mu(k)$ is the absorption coefficient and $\mu_0(k)$ is the absorption of the isolated atom. The wave

number k of the ejected photoelectron is given by the de Broglie relation $\hbar^2 k^2 / 2m = E - E_K$, where m is the electron rest mass, E is the absorbed photon energy and E_K is the energy of the K edge. The basic EXAFS formula for a single reflection in the plane-wave approximation is given by⁴

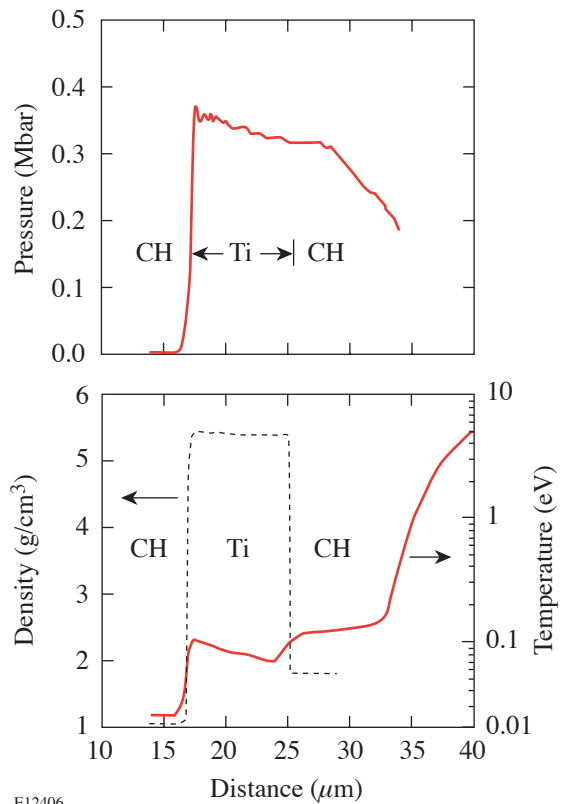
$$\chi(k) = \sum_j N_j S_0^2 F_j(k) \exp[-2\sigma^2 k^2 - 2R_j/\lambda(k)] \times \sin[2kR_j + \phi_j(k)] / kR_j^2, \quad (1)$$

where N_j is the number of atoms in the j -th shell, that is, the number of atoms surrounding the absorbing atom at a distance R_j , and $\lambda(k)$ is the electron mean free path for collisions. *FEFF8* uses the scattering potential to calculate the amplitude and phase shift of the photoelectron waves scattered from several shells of neighboring atoms including multiple-scattering paths. The total $\chi(k)$ is constructed in the curved-wave approximation (i.e., the assumption of plane wave is removed) and iteratively fitted to the experimental $\chi(k)$. The main fitting parameters are the nearest-neighbor distance R and the vibration parameter σ^2 appearing in the Debye–Waller term. R yields the density or compression if we assume three-dimensional compression. The agreement of the resulting compression with the value derived from the shock-speed measurement justifies this assumption. The vibration



E12407

Figure 97.17 One-dimensional shock profiles versus position calculated by the hydrodynamic code *LASNEX* for the instant when the shock has just traversed the V layer, assuming an incident laser intensity of ~ 0.5 TW/cm² in a 3-ns square pulse.



E12406

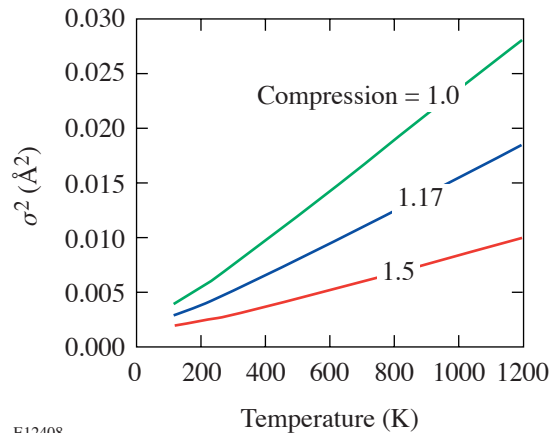
Figure 97.18 One-dimensional shock profiles versus position calculated by the hydrodynamic code *LASNEX* for the instant when the shock has just traversed the Ti layer, assuming an incident laser intensity of ~ 0.5 TW/cm² in a 3-ns square pulse.

amplitude σ^2 depends mainly on the temperature but also on the compression. σ^2 is calculated as a function of temperature, using the Debye model¹⁵ for the phonon density of states, including correlation between the motions of the absorbing and neighboring atoms; σ^2 depends on the density through the Debye temperature. The density dependence of the Debye temperature was calculated using an empirical model.⁹ Figure 97.19 shows the resulting σ^2 for V as a function of temperature and compression. As seen, compression increases the amplitude of the EXAFS signal because of the decrease in σ^2 . Similar curves have been calculated for titanium. Thus, knowing the compression and σ^2 , the temperature can be derived.

Results and Analysis

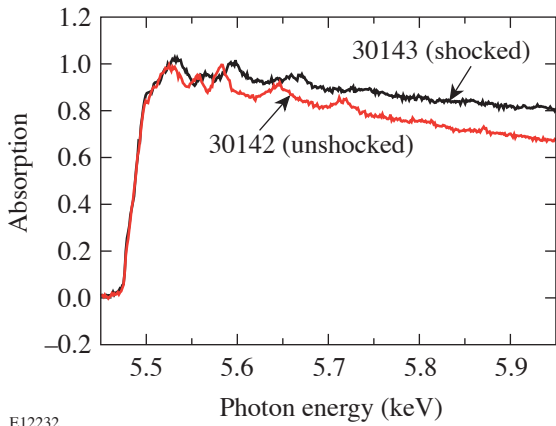
1. Vanadium

The measured absorption spectra from V are shown in Figs. 97.20 and 97.21. Figure 97.20 shows the total absorption curve in V, with and without shocking. The frequency of the



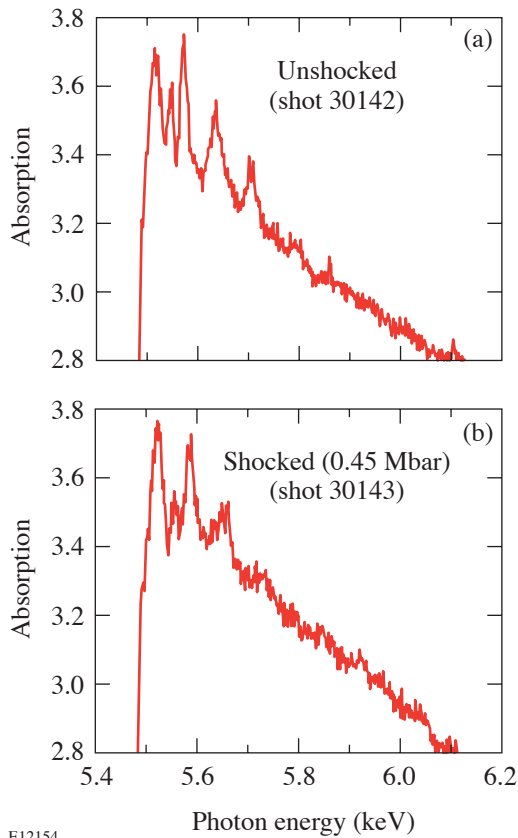
E12408

Figure 97.19 Calculated σ^2 due to thermal vibrations for V from a correlated Debye model.



E12232

Figure 97.20 Measured absorption in V (normalized to 1), with and without shocking. The lengthening of the period of EXAFS modulation in the shocked case is evidence for compression. The shock pressure was 0.45 Mbar.

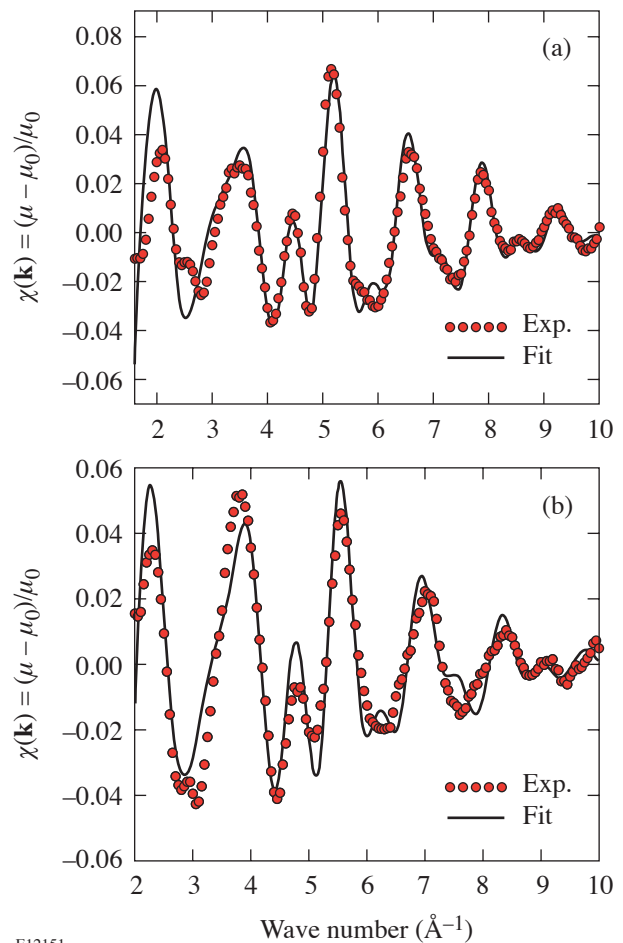


E12154

Figure 97.21 Expanded view of the EXAFS modulations in V shown in Fig. 97.20 for the unshocked case (a) and the shocked case (b). The modulations are clearly seen to decay faster when the V is shocked, due to the increased temperature. This comparison demonstrates the usefulness of EXAFS spectra in measuring the temperature of shocked metals.

EXAFS oscillations is seen to become smaller when the shock is applied. Since that frequency (in k space) is proportional to the distance R to the nearest neighbors [see Eq. (1)], the lowering of the frequency indicates a smaller R , thus a shock compression. Figure 97.21 shows a magnified view of the EXAFS modulations for the unshocked case (a) and the shocked case (b). The modulations are clearly seen to decay faster when the vanadium is shocked, due to the increased temperature. *This comparison demonstrates the usefulness of EXAFS spectra in measuring the temperature of shocked metals in the range of $T \sim 10$ to 100 meV.*

The results of fitting the V EXAFS spectra with the FEFF8 code¹⁴ for the unshocked and shocked cases are shown in Fig. 97.22. For the unshocked case, the fitting parameters were (for the first shell) $R = (2.585 \pm 0.008) \text{ \AA}$ and $\sigma^2 = (0.0111 \pm 0.0006) \text{ \AA}^2$. In the vanadium crystal (body-centered



E12151

Figure 97.22 Fitting the measured V EXAFS spectra for the unshocked case (a) and the shocked case (b) with the FEFF8 code.

cubic), the first shell has eight atoms at a distance of $(3/5)^{1/2}a$, where the crystallographic parameter a is 3.02 Å, yielding for the nearest neighbors a distance of 2.615 Å. Thus, the R found here is smaller than the expected value by ~ 0.03 Å; interestingly, the value found for R (vanadium) in V EXAFS synchrotron experiment¹⁶ was also 2.58 Å, in agreement with our value. From the measured value of σ^2 , we derive (using Fig. 97.19) the temperature 530 ± 25 K. The increase of ~ 130 K over room temperature is due to the radiation heating caused by the imploding target.

For the shocked case, the fitting parameters (for the first shell) were $R = (2.570 \pm 0.013)$ Å and $\sigma^2 = (0.0157 \pm 0.0011)$ Å². Comparing R for the unshocked and shocked cases, we derive a volume compression of $(2.585/2.570)^3 \sim 1.15$. The value of σ^2 results in a temperature of 900 ± 70 K. This increase in temperature includes the effect of radiation heating; the net temperature due to the shock alone is 770 ± 70 K.

Table 97.I summarizes the measured and computed parameters for the shocked-V experiment. EXAFS results indicate a weaker shock than predicted by *LASNEX*, but they are in agreement with the shock-speed measurement (as seen by the compression values). The measured values are accompanied by their uncertainties, whereas the *LASNEX* values are accompanied by their ranges in the axial direction. The uncertainty in the EXAFS measurement is determined by the fitting procedure and is smaller than the axial or the lateral non-uniformities described above. The EXAFS-derived values relate to the average over the shock volume. Likewise, the compression in the last column of Table 97.I is derived from the shock speed averaged (laterally) over the streak record, and its uncertainty is smaller than the range of variation in the speed.

2. Titanium

Phase transformations in shocked metals can be measured by a discontinuity in the Hugoniot curves or directly by x-ray diffraction. EXAFS can indicate a phase transformation if the Debye–Waller factor σ^2 undergoes an abrupt increase.¹⁷ This can occur if the transformation is to a disordered state or if the nearest-neighbor distances in the new crystal are disparate and

the beating of the frequencies corresponding to the various distances causes a stronger modulation damping. Shocked titanium (at much longer duration than here) is known to undergo an α -Ti to ω -Ti phase transformation at a pressure in the range of 0.029 to 0.09 Mbar, depending on sample purity.^{6,7} The pressure in this experiment is well above this range. It is not known, however, whether the transformation can occur on the nanosecond time scale. Figure 97.23 shows the EXAFS spectra from Ti, before (a) and after (b) being compressed with an ~ 0.5 Mbar shock. The experimental conditions were the same as in the vanadium experiment except

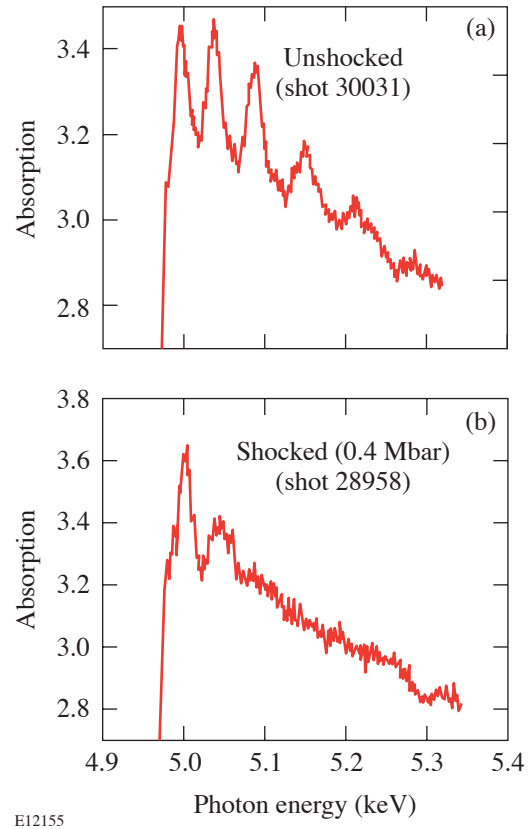


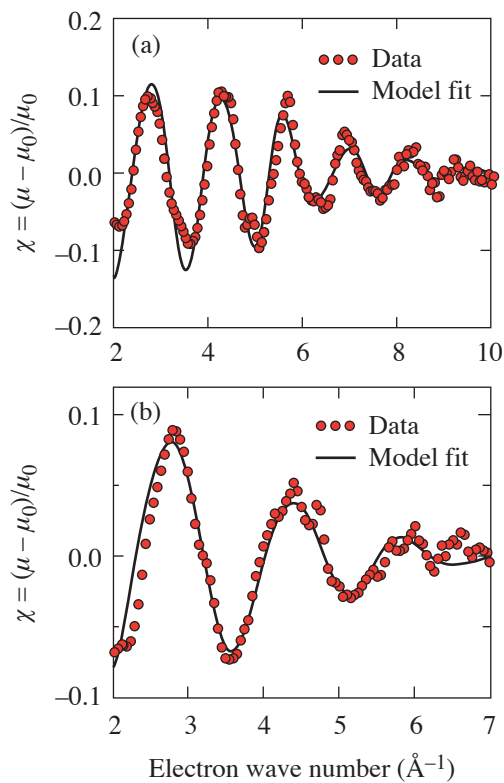
Figure 97.23 EXAFS spectra from Ti, before (a) and after (b) being compressed by a ~ 0.5 Mbar shock. The modulation with shocking is seen to be strongly damped. This is shown to reflect an α -Ti to ω -Ti phase transformation.

Table 97.I: *LASNEX*-calculated and measured parameters for shocked vanadium.

LASNEX Parameter Ranges		EXAFS Measurement		Shock-Speed Measurement
Compression	Temperature	Compression	Temperature	Compression
1.19±0.05	980±160 K	1.15±0.01	770±70 K	1.15±0.06

that the laser intensity was 0.5 TW/cm^2 . As in the case of vanadium (Fig. 97.20), the EXAFS modulations in the shocked case have a lower frequency than in the unshocked case, indicating shock compression. However, the modulations in the shocked case are seen to be much more strongly damped than in the case of vanadium. This is shown below to reflect an α -Ti to ω -Ti phase transformation.

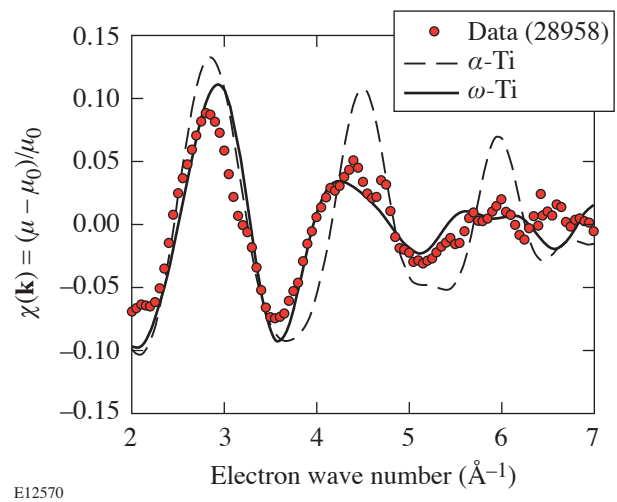
Figure 97.24 shows the fitting of the FEFF8 EXAFS code to the measured Ti EXAFS spectra taken before (a) and after (b) the shock, assuming α -Ti for both. The first-shell fitting parameters result in a volume compression of 1.2 ± 0.03 . This compares well with the *LASNEX* value of 1.2 ± 0.06 , but the error is much larger than for vanadium. The σ^2 value of the unshocked case is 0.0088 \AA^2 , which corresponds to a temperature of 380 K. For the shocked case, $\sigma^2 = 0.029 \pm 0.008 \text{ \AA}^2$, which corresponds to a temperature of $T = 2100 \pm 570 \text{ K}$. The obtained temperature is in sharp disagreement with the *LASNEX*-predicted value ($\sim 900 \text{ K}$). This strongly suggests that the large



E12409

Figure 97.24
Fitting the FEFF8 EXAFS code to the measured Ti EXAFS spectra taken before (a) and after (b) being compressed by a $\sim 0.5 \text{ Mbar}$ shock, assuming α -Ti phase.

σ^2 value is not due to a high temperature but due to a structural rearrangement such as a phase transformation. The large fitting errors also suggest that the assumed crystal structure (*hcp*) is not the correct structure for the shocked titanium. These conclusions are supported by the good agreement between measurements and simulation for comparable shocks in vanadium (Fig. 97.22), where no phase transformation is expected. In fact, whereas each α -Ti atom has six equidistant neighbors, ω -Ti atoms have two possible atomic environments:⁶ at site A there are 15 neighbors at two different distances, and at site B there are 11 neighbors at three different distances. Different distances translate to different EXAFS frequencies that, through beating, cause enhanced damping. Figure 97.25 shows this to be the case. Here FEFF calculations assuming the ω -Ti crystal structure, averaging over sites A and B, were carried out for the *LASNEX*-predicted temperature of 900 K. Only the compression was adjusted to fit the experiment, and the resulting value of 1.23 is close to the predicted value of 1.2. It should be noted that the α -Ti to ω -Ti phase transformation entails an $\sim 2\%$ volume compression.⁷ Also shown is the FEFF calculation for the α -Ti phase, using the *LASNEX*-predicted temperature and adjusting the compression to agree with the data. Figure 97.25 clearly shows that assuming the ω -Ti phase agrees with the experiment much better than assuming the α -Ti phase. Thus, the damping is dominated by the crystal structure of ω -Ti rather than by the temperature.



E12570

Figure 97.25
Fitting the FEFF8 EXAFS code to the measured Ti EXAFS spectrum, assuming the α -Ti phase (the *hcp* phase at normal conditions) and the ω -Ti phase. Only the compression was adjusted (to fit the frequency of modulation) and the *LASNEX*-predicted temperature $T = 900 \text{ K}$ was assumed.

A critical test of the assumption of phase transformation can be obtained by repeating the measurement for successively weaker shocks. Figure 97.26 shows the transmitted spectrum from a Ti sample for four different values of laser intensity (volume-averaged pressures from *LASNEX* are indicated). The reduction of the intensity by a factor ~ 2 to 0.23 TW/cm^2 shows no significant change in the spectrum. This clearly proves that the high damping rate is not due to a high temperature. At an intensity of $\sim 0.12 \text{ TW/cm}^2$ (corresponding to a pressure of $\sim 0.12 \text{ Mbar}$) the damping rate is intermediate between the unshocked and shocked cases. Thus, the results are consistent with a phase transformation occurring, very roughly, around 0.12 Mbar .

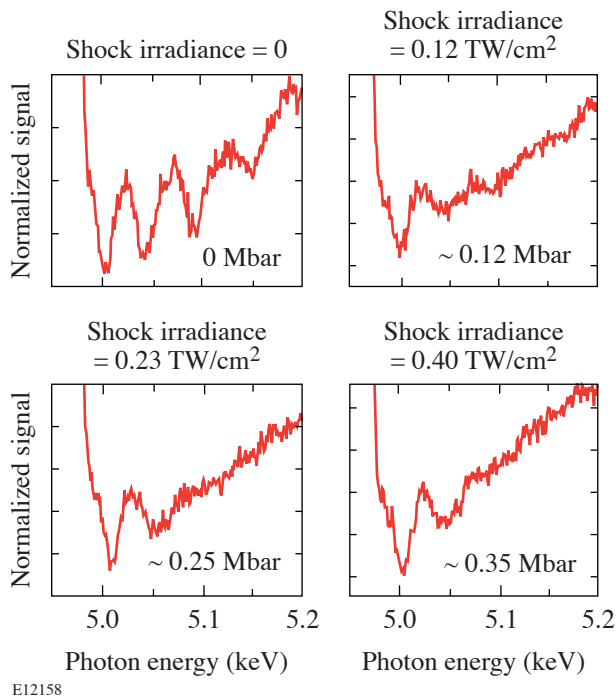


Figure 97.26 Transmitted intensity from the Ti sample for four different values of laser intensity (average pressure values from *LASNEX* are also shown). The comparison indicates that a phase transformation occurs for laser intensity of $\sim 0.12 \text{ TW/cm}^2$, which corresponds to a pressure of $\sim 0.12 \text{ Mbar}$.

Laser-shocked monocrystalline silicon was found¹⁻³ to compress uniaxially, at least during the $\sim 5\text{-ns}$ time scale of the diffraction measurement. The question arises as to whether the fast damping of the Ti EXAFS spectrum could be the result of such elastic (1-D) compression, where the varied neighbor distances would lead to beating of the corresponding EXAFS frequencies. To address this question we calculated the first-shell Ti EXAFS spectrum under the assumption of 1-D com-

pression for $\alpha\text{-Ti}$. The result is compared in Fig. 97.27 with a calculated first-shell EXAFS curve for a 3-D compression as well as with the experimental result (in Ti the contribution of more-distant shells is relatively small). The assumed 1-D and 3-D compressions (both for $T = 900 \text{ K}$) were adjusted to yield agreement between the measured and calculated EXAFS modulation frequency. In each case the coordinates of a cluster of atoms around the absorbing atom were adjusted to reflect the assumed compression. The ratio R_0/R is the reduction in distances in the direction of shock propagation (in the 1-D case). In the case of 1-D compression, the results depend on the direction of compression with respect to the atomic planes, whose orientation is different for each crystallite of the poly-

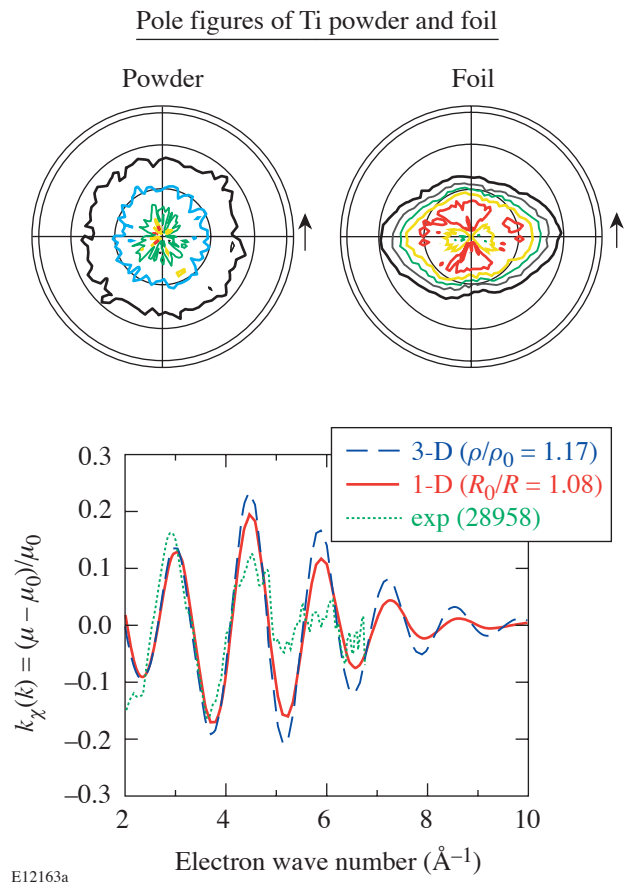


Figure 97.27 Demonstration that the fast damping of EXAFS from shocked Ti is not due to a 1-D compression. The calculated 1-D compression in $\alpha\text{-Ti}$ (in the polycrystalline sample) was averaged over all directions of (0002) poles in space, weighted by the measured pole figure of the Ti sample. The latter was normalized to the pole figure of an equivalent powdered-Ti sample.

crystalline sample. To account for this, we measured the pole figure of a Ti sample (Fig. 97.27, labeled “foil”), i.e., the statistical distribution map of the normals (or poles) to the (0002) basal planes. Since the pole-figure measurement of this distribution has an instrumental component, we corrected the result by deconvolving the measured pole figure of a powdered, i.e., an isotropically distributed, Ti sample (see Fig. 97.27). The 1-D curve in Fig. 97.27 was obtained by averaging the EXAFS spectrum of the compressed cluster over all pole directions in space, weighted by the pole figure (normalized as explained above). Figure 97.27 shows that 1-D compression does increase the EXAFS damping rate but not nearly enough to explain the measurements. We therefore conclude that the observed high damping rate in shocked Ti is very likely due to the α -Ti to ω -Ti phase transformation. Furthermore, the agreement of compression in Ti and V deduced from shock-speed and EXAFS measurements indicates 3-D compression, since the latter has been assumed in order to arrive at a compression value from the EXAFS results.

ACKNOWLEDGMENT

The pole figures obtained by Prof. S. Burns are gratefully acknowledged. This work was supported by the U.S. Department of Energy Office of Inertial Confinement Fusion under Cooperative Agreement No. DE-FC03-92SF19460, the University of Rochester, and the New York State Energy Research and Development Authority. The support of DOE does not constitute an endorsement by DOE of the views expressed in this article.

REFERENCES

1. D. H. Kalantar *et al.*, Phys. Plasmas **7**, 1999 (2000); D. H. Kalantar *et al.*, Phys. Plasmas **10**, 1569 (2003).
2. L. Loveridge-Smith, A. Allen, J. Belak, T. Boehly, A. Hauer, B. Holian, D. Kalantar, G. Kyrala, R. W. Lee, P. Lomdahl, M. A. Meyers, D. Paisley, S. Pollaine, B. Remington, D. C. Swift, S. Weber, and J. S. Wark, Phys. Rev. Lett. **86**, 2349 (2001).
3. P. A. Rigg and Y. M. Gupta, Phys. Rev. B, Condens. Matter **63**, 094112 (2001).
4. P. A. Lee *et al.*, Rev. Mod. Phys. **53**, 769 (1981).
5. T. R. Boehly, R. S. Craxton, T. H. Hinterman, J. H. Kelly, T. J. Kessler, S. A. Kumpan, S. A. Letzring, R. L. McCrory, S. F. B. Morse, W. Seka, S. Skupsky, J. M. Soures, and C. P. Verdon, Rev. Sci. Instrum. **66**, 508 (1995).
6. S. K. Sikka, Y. K. Vohra, and R. Chidambaram, Prog. Mater. Sci. **27**, 245 (1982).
7. C. W. Greeff, D. R. Trinkle, and R. C. Albers, J. Appl. Phys. **90**, 2221 (2001).
8. B. Yaakobi, F. J. Marshall, T. R. Boehly, R. P. J. Town, and D. D. Meyerhofer, J. Opt. Soc. Am. B **20**, 238 (2003).
9. R. M. More *et al.*, Phys. Fluids **31**, 3059 (1988).
10. R. W. Eason *et al.*, J. Phys. C, Solid State Phys. **17**, 5067 (1984).
11. B. A. Shiwai *et al.*, Laser Part. Beams **10**, 41 (1992).
12. P. M. Celliers *et al.*, Appl. Phys. Lett. **73**, 1320 (1998).
13. G. B. Zimmerman and W. L. Kruer, Comments Plasma Phys. Control. Fusion **2**, 51 (1975).
14. J. J. Rehr, R. C. Albers, and S. I. Zabinsky, Phys. Rev. Lett. **69**, 3397 (1992).
15. E. Sevilano, H. Meuth, and J. J. Rehr, Phys. Rev. B, Condens. Matter **20**, 4908 (1979).
16. G. Hug *et al.*, Ultramicroscopy **59**, 121 (1995).
17. A. Yoshiasa *et al.*, J. Synchrotron Radiat. **6**, 43 (1999).